Direct molecular level characterization of different heterogeneous freezing modes on mica – Part 1

Ahmed Abdelmonem[1]

[1]Institute of Meteorology and Climate Research – Atmospheric Aerosol Research (IMKAAF), Karlsruhe Institute of Technology (KIT), 76344 Eggenstein-Leopoldshafen, Germany

Correspondence to: Ahmed Abdelmonem (ahmed.abdelmonem@kit.edu)

Abstract. The mechanisms behind heterogeneous ice nucleation are of fundamental importance to the prediction of the occurrence and properties of many cloud types, which influence climate and precipitation. Aerosol particles act as cloud condensation and freezing nuclei. The surface–water interaction of an ice nucleation particle plays a major, not well explored, role in its ice nucleation ability. This paper presents a real–time–molecular–level comparison of different freezing modes on the surface of an atmospherically relevant ~~metal oxide~~mineral surface (mica) under varying supersaturation conditions using second harmonic generation spectroscopy. Two sub-deposition nucleation modes were identified (one- and two-stage freezing). The nonlinear signal at water-mica interface was found to drop upon the formation of a thin film on the surface regardless of 1) the formed phase (liquid or ice) and 2) the freezing path (one– or two–step), indicating similar molecular structuring. The results also revealed a transient phase of ice at water–mica interfaces during freezing, which has a lifetime of around one minute. Such information will have a significant impact on climate change, weather modification, and tracing of water in hydrosphere studies.

1 Introduction

Clouds influence the energy budget by scattering sunlight and absorbing heat radiation from the earth and are therefore considered the major player in the climate system. Formation of ice changes cloud dynamics and microphysics because of the release of latent heat and the Bergeron-Findeisen process, respectively (Pruppacher and Klett, 1997). Ice nucleation in the atmosphere can be triggered heterogeneously by aerosol particles, ice-nucleating particles (INP), or occurs homogeneously at about -38°C (Pruppacher and Klett, 1997). Cloud evolution depends not only on temperature and humidity, but also on the abundance and surface characteristics of atmospheric aerosols. Understanding the factors that influence ice formation within clouds is a major unsolved and pressing problem in our understanding of climate (Slater et al., 2016). Field and laboratory experiments on cloud formation started decades ago (see (Schaefer, 1949; DeMott et al., 2011; Hoose and Mohler, 2012) and references therein) and are ongoing. A wide variety of results and observations has been obtained in cloud microphysics, especially with respect to the ice nucleation ability of atmospheric aerosol particles and, hence, the mechanisms of cloud dynamics, precipitation formation, and interaction with incoming and outgoing radiation. Aerosol particles act as cloud condensation nuclei for liquid clouds, immersion or contact freezing nuclei for mixed-phase clouds, and heterogeneous deposition nuclei for ice (cirrus) clouds. Depending on whether water nucleates ice from the vapor or the supercooled liquid phase, ice nucleation is classified as deposition nucleation or immersion nucleation, respectively. Despite numerous investigations aimed at characterizing the effect of particle size and surface properties of the INP, there is a lack of information about the restructuring of water molecules on the surface of INPs around the heterogeneous freezing point.

In this paper, discrimination between different modes of freezing of water on an ice-nucleating surface using nonlinear optical spectroscopy is demonstrated. Mica, a widely spread layered clay mineral and one of the most prominent mineral

surfaces due to its atomic flatness and chemical inertness produced by perfect cleavage parallel to the 001 planes (Poppa and Elliot, 1971), was selected as a model surface in this study. However, the image of an inert and atomically smooth surface prepared by cleavage of muscovite mica in an ambient atmosphere is not quite correct (Christenson and Thomson, 2016). Surface analytical techniques found that the surface of muscovite mica cleaved in laboratory air, as the case in this work, contains a water-soluble compound, almost potassium carbonate crystallites, which may cover few tenths of a percent of the surface area (Christenson and Israelachvili, 1987). Nevertheless, definitive chemical analysis showing its presence is not yet available. However, the mobility of the potassium ions as potassium carbonate does not necessarily affect significantly any measurement of average surface properties as in the case of this work, and at high humidities the potassium will be widely dispersed across the surface. The readers which are interested in more details on the nature of the mica surface in general and air-cleaved mica surface in particular are referred to the review paper of Christenson, H. K. and Thomson, 2016 and papers cited therein.

Mica, as natural particles, is believed to be among the most effective ice nucleating minerals in the deposition mode (Eastwood et al., 2008; Mason and Maybank, 1958). An early study, using a projection microscope, of deposition nucleation of ice on freshly cleaved synthetic fluorophlogopite mica, which is similar in structure to muscovite but has the hydroxyl groups replaced by fluorine, using a projection microscope, revealed that there is no growth of ice until saturation with respect to water is reached (Layton and Harris, 1963). The authors concluded that at temperatures above -40 °C, the growth of ice on mica should be a two-step process: A nucleus forms as water and then freezes. Experimental evidence of two-step nucleation was also provided by (Campbell et al., 2013) using an optical microscope. With the help of a scanning optical microscope, they showed that the nucleation, of various organic liquids crystallising from vapour on mica surfaces, favored specific nucleation sites with surface features such as cleavage steps, cracks and pockets. However, they suggested that a supercooled liquid phase forms first and then freezes after it has grown to a size which thermodynamically favors the solid phase. These assumptions were based merely on thermodynamic observations (temperature and vapor supersaturation). A later study by the same group, has confirmed the role of the surface features and the two-step process for the organic liquids, and strongly suggested a two-step process for water and ice. Recent MD simulations of deposition freezing revealed that water first deposits in the form of liquid clusters and then crystallizes isothermally from there (Lupi et al., 2014). So far, there has been no direct experimental evidence of two-step freezing based on probing the molecular structuring of water molecules next to the surface.

In this work, second-harmonic generation (SHG) in total internal reflection (TIR) geometry was used to probe the change in the degree of ordering of water on the surface of mica. SHG is a powerful and simple, compared to sum-frequency generation (SFG), surface−sensitive spectroscopic tool for studying molecules near surfaces and at interfaces (Shen, 1989b; Shen, 1989a). The amplitude and polarization of the generated field, as a function of the polarization of the incident fields, carry information on the abundance and structure of the interfacial molecules between two isotropic media (Jang et al., 2013; Rao et al., 2003; Zhuang et al., 1999). More details on SHG and SFG can be found in the experimental section and in SI. In the system described here, the SHG signal is originated from the the nonresonant OH stretching vibrations at the interface electric dipolar contribution of the interfacial molecules. The signal response relates to the overall arrangements of the interfacial entities (Fordyce et al., 2001; Goh et al., 1988; Luca et al., 1995) and propotional to the incident field and the second-order nonlinear susceptibility $\chi^{(2)}$ of the interface. When the interface is charged the static electric field due to the charge can induce a third-order nonlinear polarization due to the contribution of the third-order nonlinear susceptibility $\chi^{(3)}$ of the solution (Ong et al., 1992; Zhao et al., 1993). In this work, the contribution of $\chi^{(3)}$ to the total SHG signal has been ignored because there was no significant change in the interface charge with temperature. The change of pH with temperature is very trivial for neutral water (e.g. from pH 7 at 25 °C to pH 7.47 at 0 °C). In addition, this change does not mean that water becomes more alkaline at lower temperatures because in the case of pure water and according to the Le Châtelier's principle there are always the same concentration of hydrogen and hydroxide ions and hence, the water is still

neutral (pH = pOH) even if its pH changes. The pH 7.47 at 0°C is simply the new reference of neutral water pH at 0 °C. In addition, assuming that the surface potential has an influence on the background signal, this will not change even if the pH changes with temperature because the surface potential values of the muscovite basal plane (the surface under study) is pH independent in the range from pH 5.6 to 10 (Zhao et al., 2008)More details of SHG and SFG can be found in SI.

5　The results provide new insight into heterogeneous freezing processes and show the suitability of the method for studying current issues relating to ice nucleation, which will contribute to its rapid development in the next years. Initially, I found that the SHG signal drops upon the formation of a thin film regardless of whether the freezing path consists of one− or two−steps and the initially formed phase, liquid or ice, indicating a similar molecular structuring. In addition, I observed a transient SHG signal after immersion freezing.

10　The hygroscopicity of mica is expected to play a ruole in the described processes. The hygroscopicity and Langmuir isotherm studies on mica are available in literature but only at room temperature where the sample and environment are at equilibrium (Balmer et al., 2008; Beaglehole et al., 1991; Hu et al., 1995). Such studies at supercooled surfaces are worth to do and could be a topic of future work. An AFM study at 21 °C showed no water absorbed on the surface of mica at RH = 18 % (Hu et al., 1995). The first uniform water phase, of large two-dimensional islands with geometrical shapes in epitaxial

15　relation with the underlaying mica lattice, was observed at RH = 28 %. The growth of this water phase is completed when the humidity reaches 40 to RH = 50 %. In my experiments on mica it is not possible to detect sub-monolayers, at least at this stage, due to technical reasons mentioned later. In the presented work, only clear steps in the signal were considered.

2 Experimental

2.1 Materials and setup

20　All experiments were carried out using MilliQ water (18.2 MΩ·cm). The total organic content in this water is below 4 ppb. Mica samples were obtained from Plano GmbH, Germany. The mica samples were freshly cleaved parallel to the 001 plane in air right before use. The freshly cleaved mica exhibits a wetting surface (on which water was spreading visually). The SHG experiments were conducted using a femtosecond laser system (Solstice, Spectra Physics) with a fundamental beam of 800 nm wavelength, 3.5 mJ pulse energy, ~80 fs pulse width, 1 kHz repetition rate, and a beam diameter of ~2 mm at the

25　interface. The supercooled SHG setup and the measuring cell wereare similar to those described in previous publications (Abdelmonem et al., 2015; Abdelmonem et al., 2017). Compared to the setup described in (Abdelmonem et al., 2015), a single fundamental beam incident on the interface was used, Fig. 1, and the SM (S-polarized SHG / 45°-polarized incident) polarization combination was measured. Figure 1 shows the sample and beam geometry. The polarization direction of the incident beam was controlled by a half-wave plate followed by a cube polarizer. The generated signal was collected using a

30　photomultiplier tube (PMT) placed downstream of an optical system including band pass filters for 400 nm and a polarization analyzer. Briefly, in the SHG experiments aA sapphire prism iswas used as an optical coupler to the surface of a thin mica substrate, the basal plane of which iswas exposed to liquid water or water vapor. The fundamental beam had an incident angle of 15° with the surface normal of the outer side of the prism. Under this geometry, the reflected fundamental (800 nm) and generated SHG (400 nm) beams co-propagate to the sapphire-air interface at the other side of the prism at

35　which both beams are refracted at two different angles. Only the SHG signal was allowed to reach the detection path. Before starting the measurements, the polarization of the SHG signal generated from water at the surface was analyzed and found to have the expected maxima at S and P polarizations corresponding to an incident 45°-polarized light. The signal was quadratically dependent on the input power. To study mica in TIR geometry, an index matching gel (IMG) from Thorlabs (G608N3, RI~1.45186 at 800nm) wasis used to fix the mica sample on the hypotenuse of the sapphire prism. The freezing

40　point was not specified by the manufacturer but tested in the lab. At least the gel was not frozen until -45 °C. A detailed description of sample geometry and the selection of the IMG was published in (Abdelmonem et al., 2015). Less than 15% of

the laser output power was coupled to the setup to not destroy the IMG. The fluctuation in the signal due to reducing the laser power limited the sensitivity of the system and it was not possible to monitor minor changes which may arise from pre-adsorption of sub-monolayers at temperatures higher than the dew point or freezing point.
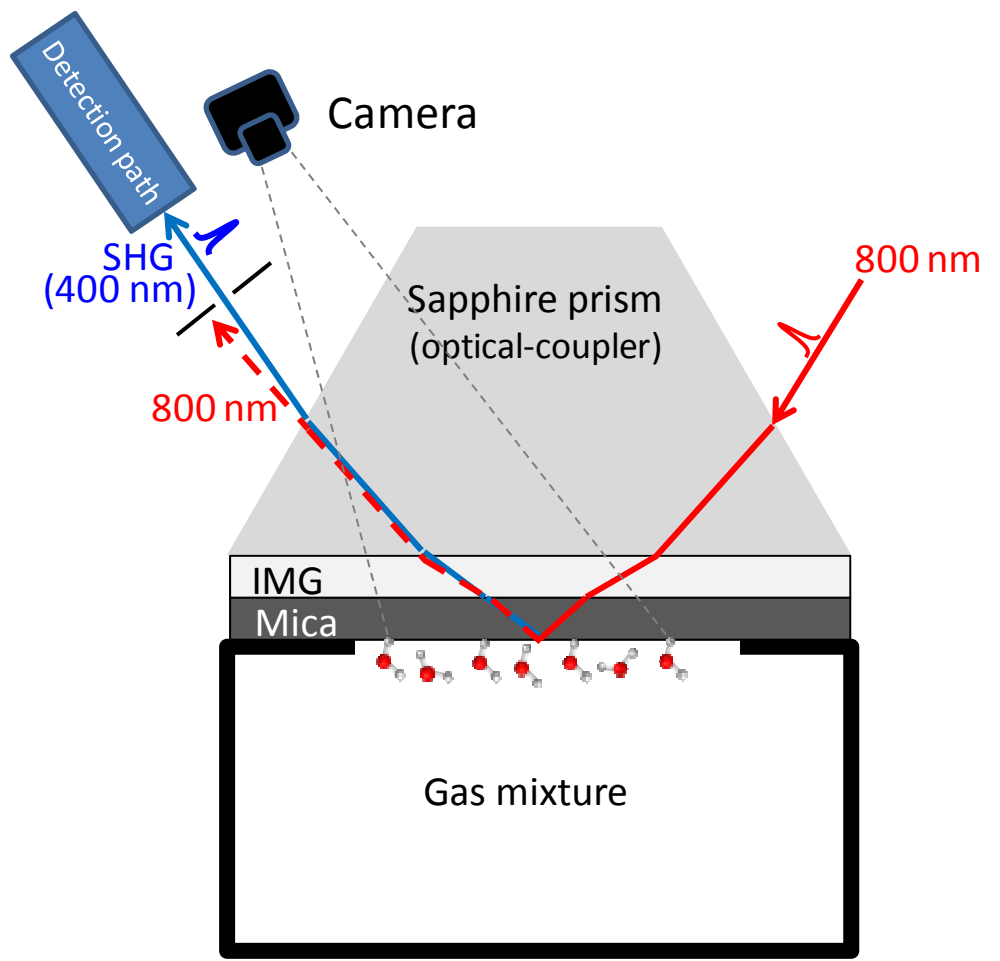

Figure 1: The sample and beams geometry. See text for details

A homemade temperature-controlled environmental chamber, Fig. 2, was integrated into the setup to control the sample temperature. A commercially available cold-stage (Linkam model HFS-X350) was used after modifying the housing to accommodate the SHG setup. The sapphire prism was place in a cupper adaptor which was fixed on the silver block of the Linkam cold-stage. The substrate of interest was sealed to a circular opening of 8 mm in diameter in a teflon cell which was being purged with the sample gas during the experiments. The cold-stage can perform controlled heating and cooling ramps, applied to the silver block, at rates between 0.01 and 100 °C/min. Temperature stability of the cold-stage is better than 0.1 K. The temperatures of the air inside the cell and the sapphire prism top and bottom were measured using four-wire-Pt100 elements. The temperature of the probed spot on the surface was considered to be the average of the sample top and sample bottom temperatures. However, it should be emphasized that the exact onset condition of freezing is not the focus of this work, but rather the study of the qualitative behavior of water molecules during freezing on the different paths. During the experiments, the gas box was filled with N_2 gas to avoid condensation on the outer surfaces of the prism during cooling. The humid air pumped to the measuring cell was obtained by mixing dry gas and 100 % humid gas with different ratios at 21 °C using two mass flow controllers (Tylan 2900). The continuous flow of the gas (either dry or humid) during the experiment set the temperature inside the cell to 21 °C ± 0.5 °C. The corresponding fluctuation of the relative humidity was less than 0.2%. The corresponding fluctuation in the dew point, at RH = 5 ±0.2 for instance, was ±0.5 °C. The gas mixing ratio versus RH was calibrated by setting a mixing ratio, cooling the sample and recording the condensation/freezing temperature at

which the reflectivity at an angle equals to the critical angle of TIR for air-mica interface starts to drop due to the violation of TIR condition. This temperature was used to define the corresponding RH using Arden Buck equation.

The same method was used to differentiate between liquid-film, liquid-bulk, transient ice, and stable ice in this work. The border between a film at the solid-air interface and a bulk at the solid-water (or -ice) was defined experimentally by the point where the intensity of a TIR reflected light from the solid-air interface drops due to the violation of TIR condition when the refractive index of the contact medium changes drastically from that of air (n_a=1) to one of those of water or ice ($n_{w \text{ or } i}$ > 1.3). Whether the contact medium is liquid or ice, this was defined by the change in the light scattering, observed at a CCD camera (Guppy F-036 Allied Vision Technology with LINOS Macro-CCD Lens 0.14x (1:7) f4) placed close to the detection path, Fig. 1. After immersion freezing, there was a rapid increase in the signal and then slow decrease. The maximum after the rapid increase was defined as the "transient ice" data point. After reaching a maximum, the signal was decreased with time until stabilized after certain time. This stabilized signal was defined as the "stable ice" data point.
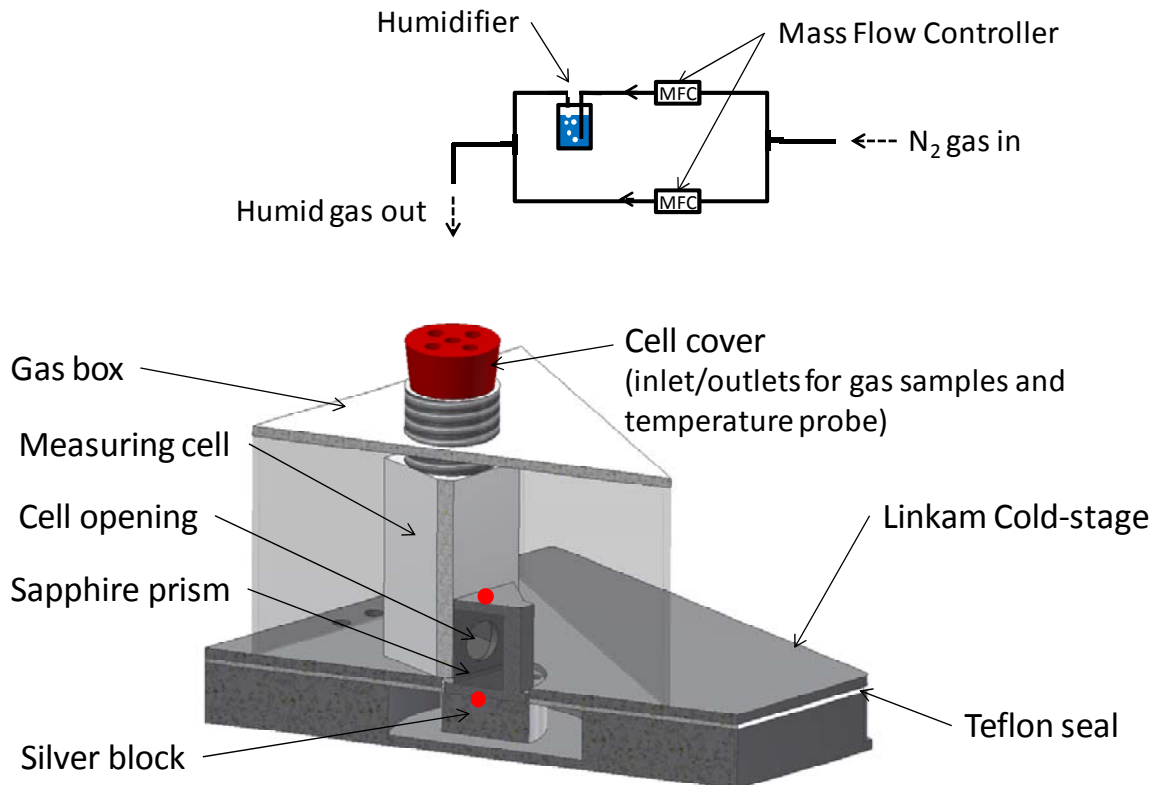

Figure 2: The temperature-controlled environmental chamber configuration, humidification and temperature sensors. The red dots are the position of the sample temperature sensors. There is a temperature sensor inside the measuring cell (not shown)

A control~~Control~~ software was developed to adhere to a predefined temperature profile and to measure the SHG signal and the temperature of the substrate. Temperature profiles were repeated several times for each sample to test reproducibility. In each run, the sample was heated to 110 °C while purging with N_2 gas (99.9999 %) to evaporate any residual water, then cooled down to 0 °C at a rate of 10 °C/min and then down to the heterogeneous freezing point at a rate of 1 °C/min. This cooling profile was the same for all runs to allow for logical comparison. An experiment with a mica-N_2 gas interface was carried out to ensure that the change in the refractive indices of the sapphire prism, IMG, and mica substrate with temperature ~~had~~ have no significant effect on the resulting SHG signal in the range of freezing temperatures ~~applied~~ observed in this work, Figure S4 in SI. ~~During the freezing experiments, the substrate of interest was sealed to a circular opening of 8 mm in diameter in a teflon cell which was purged with a dry-humid air mixture. The prism was inserted into a~~

~~tight housing of the cooling/heating stage. The temperatures of the sample top, sample bottom, and air mixture inside the cell were recorded using four wire Pt100 elements. This was not done to determine the exact onset conditions of freezing, but rather to study the qualitative behavior of water molecules during freezing on the different paths. The humidity of the gas mixture pumped to the measuring cell was adjusted by mixing N₂ gas with saturated water vapor at room temperature (21 °C). The mixing ratio was set using Tylan 2900 flow controllers.~~

~~The SHG experiments were conducted using a femtosecond laser system (Solstice, Spectra Physics) with a fundamental beam of 800 nm wavelength, 3.5 mJ pulse energy, ~ 80 fs pulse width, 1 kHz repetition rate, and a beam diameter of ~ 2 mm at the interface. Less than 15% of the laser output power was coupled to the setup to not destroy the IMG. The fluctuation in the signal due to reducing the laser power limited the sensitivity of the system to monitor minor changes which may arise from pre-adsorption of sub-monolayers at temperatures higher than the dew point or freezing point.~~

~~Compared to the setup described in (Abdelmonem et al., 2015), a single fundamental beam incident on the interface was used and the SM (S-polarized SHG / 45° polarized incident) polarization combination was measured. The polarization direction of the incident beam was controlled by a half wave plate followed by a cube polarizer. The generated signal was collected using a photomultiplier tube (PMT) placed downstream of an optical system including the appropriate filters and a polarization analyzer.~~ As mentioned above, ~~T~~the incident angle from air of the fundamental beam was adjusted to 15° with respect to surface normal of the outer side of the sapphire prism. The corresponding incident angle on the mica-air or -water interface was ~ ~~51.6~~63.4°, which is higher than the critical angles of TIR for mica-air (~ ~~34.1~~39.7°) and mica-water (~~~50.2~~59.2°) interfaces. This guaranteed a TIR condition regardless of any changes in the Fresnel factors caused by the change of refractive indices with changing temperature. The advantage of using SM polarization combination is its dependence on only one non-vanishing nonlinear susceptibility tensor element (χ_{yyz}), (Shen, 1989a; Zhuang et al., 1999), at any working angle which makes it a direct probe of the degree of order of the molecules at the interface.

The SHG signal is mainly produced by all polarizable species within the SHG-active region as long as the inversion symmetry is broken. The polarizable species at the surface of interest are the water molecules and the surface OHs. The contribution of water molecules are limited by the penetration depth inside the second medium (air, liquid water or ice). Under the optical geometry described above, the calculated penetration depths are about 130 nm, 328 nm, and 253 nm for air, liquid water bulk, and ice bulk as contact media respectively. Under the thermodynamical conditions of the presented work, the thickness of the ice (or water) layer should exceed 1 μm within 1 sec after nucleation which is far beyond the penetration depth of the evanescent field. Therefore, although the exact thickness cannot be determined in this setup it does not affect the probed signal, by the Two-Interface Problem, because the second interface (ice-air or water-air) is not within the focal volume of the pump beam and the non-resonant signal is coming exclusively from the first interface (water-solid or ice-solid). For the ice layer thickness, the reader is referred to the calculations of the growth velocity of a solidification front normal to the ice surface provided in the Supplementary Materials of the recent work of Kiselev et al. (Kiselev et al., 2016). These calculations were taken from numerous works of Libbrecht (Libbrecht, 2003; Libbrecht, 2005). For calculations of growth due to condensation, the reader is referred to the Aerosol Calculator Program (Excel) by Paul Baron which is based on equations from (Willeke and Baron, 1993; Hinds, 1999; Baron and Willeke, 2001). The signal was not collected until it became stabilized and therefore, it was assumed that the ice layer after deposition was uniform at the surface covered by the laser spot.

3 Results and discussion

The relative humidity (RH) of the purged gas was set to specific values in different runs to allow for different freezing modes on the surface of mica. Figure ~~1a~~ 3a shows the change in normalized Fresnel factor-corrected (see SI for details) SHG

intensities under SM polarization combination for deposition freezing (DF) at -38 °C (black solid line and circles), -21 °C (red solid line and empty squares), and at -12.5 °C (green solid line and empty triangles) labeled by DF1, DF2, and DF3, respectively. In DF1, the cell was filled with N_2 gas and the sample was cooled down to a temperature, -38 °C, far below the dew point at RH = 5 % (-21 °C). At -38 °C, the cell was purged with humid air of RH ~ 5 %. An ice–film formed immediately on the surface, reflected by a drop in the SHG signal compared to that of air-mica interface. In DF2 and DF3, the cell was purged continuously with humid air of RH = 5 and 11 %, respectively, and then cooled down until freezing and growth of ice were observed on the surface. Deposition freezing and the formation of an ice–film started at -21 and -12.5 °C for RH = 5 % (DF2) and 11 % (DF3), respectively. The results show a drop in the SHG signal with respect to the signal of the mica-air interface upon freezing for the three cases DF1, DF2, and DF3. However, the relative signal drop for DF1 differs from those of DF2 and DF3. DF2 and DF3 were observed at temperatures equal to the dew points at the preset RHs, indicating two-step nucleation, first condensation, and then freezing. The coincidence of the SHG signals of the thin ice–film formed in DF2 and DF3 indicates ~~identical structuring~~similar degree of order of water on the surface in two–step deposition freezing regardless of the onset temperature. This means that at temperatures above -38 °C, growth of ice on mica apparently is a two-step process: Water first condenses and then freezes. This confirms on the molecular level the two-stage nucleation hypothesis which suggests that a nucleus forms as a liquid cluster and then freezes (Layton and Harris, 1963; Lupi et al., 2014). Further pumping of the gas mixture to the measuring cell allows for the growth of the ice–film by diffusion. The resulting ice–bulk shows a further drop in the signal for DF2 and DF3. This drop was not observed for DF1, thus indicating a major difference in the spectroscopic behavior of ice between one–step and two–step deposition freezing. To ensure that the lack of change in the SHG signal after the growth of an ice–film to ice–bulk in one-stage nucleation, DF1 figure ~~1a~~3a, is not an artefact, DF1 and DF2 were compared using a different system (sapphire–water interface, Fig. ~~1b~~3b). Figure ~~1b~~3b shows the change in SHG intensity at the surface of sapphire for DF at -38 (black solid line and circles) and at -23 °C (red solid line and empty squares) labeled by DF1 and DF2, respectively. As in the case of mica, the drop in SHG intensity after the formation of an ice–film was followed by another drop upon further pumping of humid air of RH = 5 % in the two-step freezing process (DF2), but not in one-step (DF1) freezing.
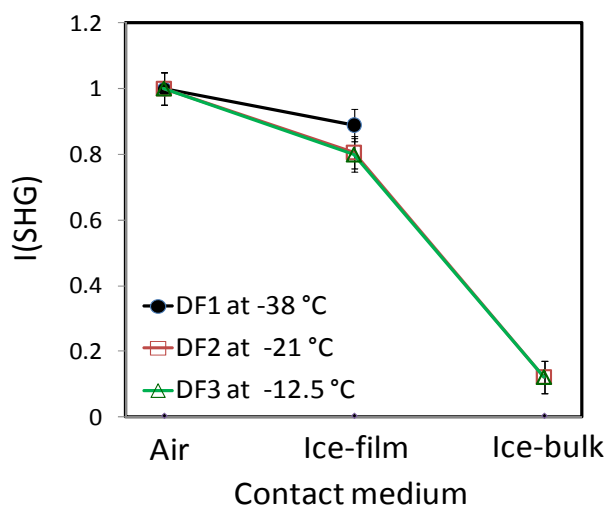
(a) Mica–ice interface
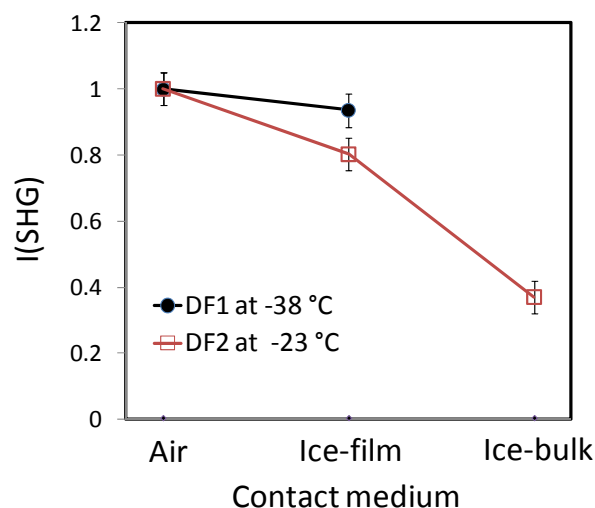
(b) Sapphire–ice interface

Figure ~~1~~3: SHG intensity measured at the surfaces of mica (a) and sapphire (b) in contact with air, ice–film, and ice–bulk, respectively, collected in SM polarization combination during the three different cooling cycles, DF1: Sample cooled down first to -38 °C under dry N_2 gas , followed by pumping water vapor of RH = 5 % to the measuring cell. DF2: Sample cooled down under flow of water vapor of RH = 5 %. DF3: Sample cooled down under flow of water vapor of RH = 10 %. The signal is Fresnel-corrected and normalized to the air value. All connection lines between points are just for guiding the eyes.

Figure ~~2~~ 4 shows three different freezing experiments at different RHs. The gas RH was adjusted to allow liquid condensation (LC) during cooling at temperatures higher than those of deposition freezing. Constant pumping of humid air at RH = 20, 30, and 40 % and cooling down resulted in the formation of stable liquid films at -3.5, 3, and 7 °C, respectively. At all RH values, the SHG signal drops down upon the formation of a liquid–film by LC. The relative drop of the signal with respect to the air signal is similar to that observed in the DF experiments, Figure ~~1a~~3a. Comparing Figures ~~1a~~ 3a and ~~2~~4, the SHG signals are in the same range regardless of the film phase (liquid or ice). By further pumping of humid air after LC, liquid–bulk forms at the surface with a signal that is lower than that of the liquid–film. This is mostly due to the contributions from the few secondary layers of the interfacial water. Further cooling of the sample in contact with liquid–bulk causes water to freeze by immersion freezing (IF). The observed IF temperatures for IF1, IF2, and IF3 are similar and center around -11 °C ± 1 °C which is within the range of IF temperatures observed for freezing of bulk water in contact with the surface of mica in former studies (Abdelmonem et al., 2015; Anim-Danso et al., 2016). IF produced a transient ice phase with SHG intensity higher than that of the interfacial water of the bulk liquid. The lifetime of the transient phase is around one minute, Figure ~~3~~5. The values of the SHG intensities plotted in Figure ~~2~~4 for transient ice–bulk are the peak values found on the transient curves shown in Figure ~~3~~5 after Fresnel factor corrections and normalization to the mica-air signal. The transient phase may have had peak values higher than those obtained from Figure ~~3~~5, but they were not detected due to the fast signal decay right after nucleation and the limited time resolution of signal detection of about 2.5 sec. A transient phase lasting for several minutes was reported very recently by Lovering et al. using SFG at a water-silica interface (Lovering et al., 2017). They suggested a transient existence of stacking-disordered (non-centrosymmetric) ice during the freezing process at water-mineral interfaces. Anim-Danso et al. also observed such transient ice lasting for a few tens of seconds in SFG experiments at a high-pH (9.8) solution-sapphire interface. They suggested that charge transfer and the stitching bilayer are perturbed at high pH, which leads to a decrease in SFG intensity. The present work shows that the transient ice occurs at neutral pH on mica surface and has a significant nonresonant component which is observable with the simple SHG technique. Apparently, the lifetime of the transient phase depends on the substrate and probably on the liquid–bulk size and might play a big role in the ice nucleation ability of the surface. However, this requires a comparative study involving different substrates, which will be subject of future work.
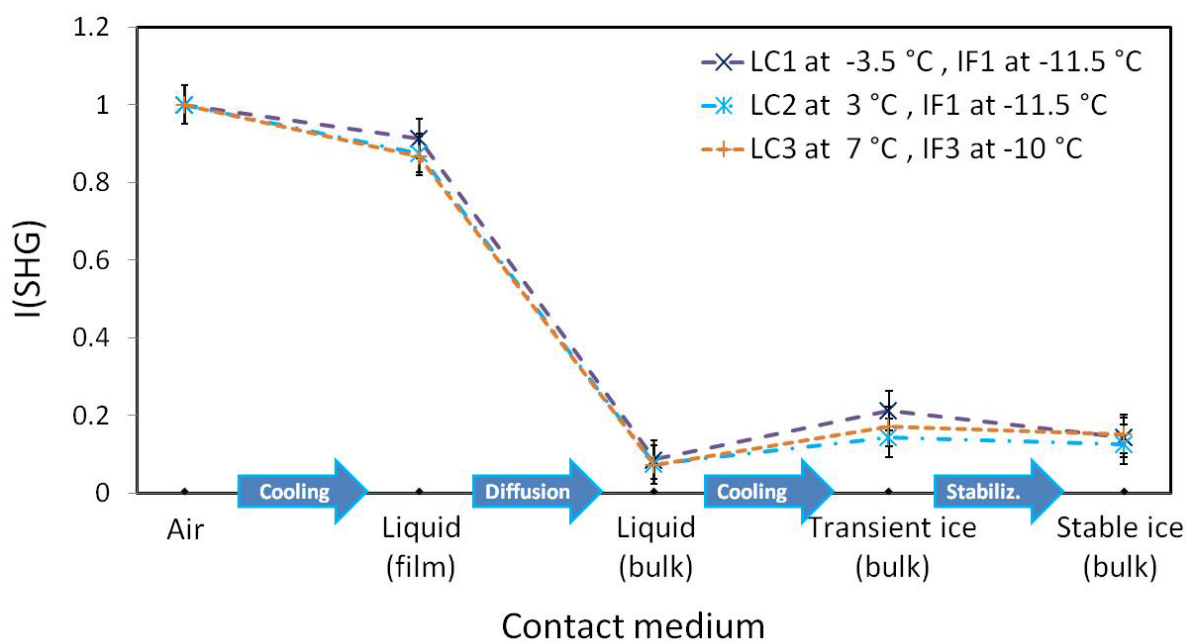

Figure ~~2~~4: SHG intensity measured at the surface of mica in contact with air, liquid–film, liquid–bulk, transient ice–bulk, and stable ice–bulk, respectively, collected in SM polarization combination during three different cooling cycles, LC1 IF1: Sample cooled down under flow of water vapor of RH = 20 %. LC2 IF2: Sample cooled down under flow of water vapor of RH = 30 %.

LC3 IF3: Sample cooled down under flow of water vapor of RH = 40 % (see text for details). The signal is Fresnel-corrected and normalized to the air value. All connection lines between points are just for guiding the eyes.
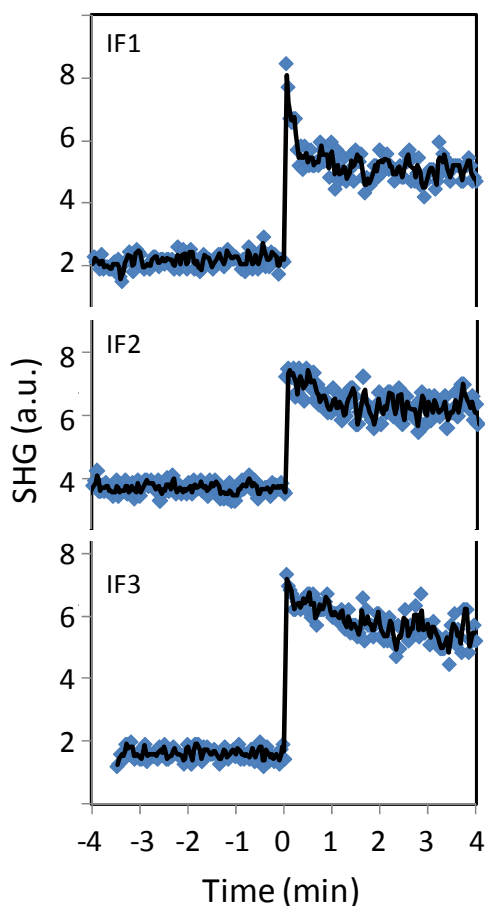
Figure 3̶5: Typical variation in the SHG intensity around the immersion freezing points for IF1, IF2, and IF3 during the cooling experiments

Finally, I would like to comment on the drop, rather than increase, of the signal upon adsorption of water (or ice) on the surface (of either mica or sapphire). Since SHG response reflects the overall arrangements of the polar entities at the interface between two isotropic media (Fordyce et al., 2001; Goh et al., 1988; Luca et al., 1995), signal intensity is expected to increase when a single (or few non-centrosymmetric) layer(s) of water or ice is(are) formed at the surface. It is clear from Figures 1̶3 and 2̶4, however, that SHG intensity decreases upon deposition freezing, condensation, and growth of liquid layers by diffusion. This can be explained by phase interference between two signals originating from two different interfacial groups of opposite dipole moments: surface-OH points out of the surface and water̶-OH points to the surface. A cleaved mica surface exhibits a disordered hexagonal arrangement of Si- (partly Al-) anddoubly coordinated O atoms in the outermost layer (Ostendorf et al., 2008). As an aluminosilicate mineral, this surface may protonate which hydrate immediately in contact with the ambient air (forming silanol and aluminol groups at the surface). In this case, .̶ T̶the mica-dry air signal can mainly originates̶ from the surface hydroxyl groups (dangling−OH) which are naturally pointing out from the surface. Since mica surface is inherently negatively charged, the interfacial water̶-OH groups will point to the surface and thus have a phase opposite to that of the surface−OH groups, as was reported by Shen and co-workers (Zhang et al., 2008) on negatively charged surfaces. This well explains the ostensible decrease in the overall signal upon deposition and condensation. When the surface of mica is covered with bulk water of a pH ~ 7, it becomes totally deprotonated (no free−OH) (Odelius et al., 1997). One in four Si in the tetrahedral layers of mica is randomly substituted for Al (Christenson and Thomson, 2016). The result is that the majority of the surface hydroxyl groups of a cleaved basal plane are silanol and therefore the surface deprotonation is significantly determined by silica. The point-of-zero-charge (pzc) of silica lies between its respective isoelectric points pH 2 – 3 (Hartley et al., 1997; Iler, 1979; Scales et al., 1992) and hence the silanols in silica

9

(Si-OH) deprotonate totally in the presence of neutral water (pH ~ 7). Under this condition the SHG signal comes exclusively from the interfacial water molecules between the surface and liquid-bulk. This defines a new reference of the signal generated at the new interface (liquid-solid rather than gas-solid). The increase of the signal afterwards indicates more structuring of either the interfacial water before freezing, like shown in (Abdelmonem et al., 2015) or the interfacial ice after freezing like shown here. It is worth to mention that, the presence of free surface hydroxyl groups on cleaved mica is poorly discussed in literature. Miranda et al. have indirectly referred to their (hydroxyl groups) existence in their work on mica-water vapor interface using SFG (Miranda et al., 1998). They used deuterated water (D_2O) in the SFG experiments to avoid confusion of the hydroxyl stretch modes in the spectrum from both water and mica. Maslova et al. have discussed it a bit explicit in their work on surface properties of cleaved mica and they assumed that hydroxyl groups of the basal plane are not reactive (Maslova et al., 2004).

Conclusion

In summary, I used a simple SHG setup to discriminate and describe three different freezing paths on the surface of mica. The results decide on, and confirm on the molecular level, the previous speculations about the existence of two-stage deposition ice nucleation at temperatures above -38 °C. One-step and two-step deposition freezing of a thin film of ice show water structure similar to that of a thin film of liquid water. When a liquid–bulk freezes at the surface by immersion freezing, there is a transient non-centrosymmetric ice phase of high non-resonant SHG signal. The lifetime of the transient phase is suggested to be substrate–dependent and expected to affect ice nucleation efficiency. The presented results open up new horizons for the role of aerosol surfaces in promoting and stabilizing heterogeneous ice nucleation. They provide novel molecular–level insight into different ice nucleation regimes using a simple spectroscopic technique. Investigating the structuring of water molecules upon freezing next to solid surfaces is crucial to many scientific areas, such as atmospheric physics and chemistry, hydrology, and environmental and industrial applications.

The work demonstrates the worthwhile of investigating different ice nucleation processes and water structuring upon freezing on the molecular-level using SHG spectroscopy. The manuscript is considered as a cornerstone of future complementary studies involving other surfaces and other techniques to precisely investigate the layer thickness, the surface morphology effect, the cooling rates ...etc. The difficulty of characterizing monolayer films rose from the use of the IMG which required reducing the power. An alternative would be to approach the surface from the air side which then has the disadvantage of a week SHG signal and Two-Interface Problem. These are challenges which will be tackled in future works.

Acknowledgements

References

Abdelmonem, A., Lützenkirchen, J., and Leisner, T.: Probing ice-nucleation processes on the molecular level using second harmonic generation spectroscopy, Atmos. Meas. Tech., 8, 3519-3526, doi: 10.5194/amt-8-3519-2015, 2015.

Abdelmonem, A., Backus, E. H. G., Hoffmann, N., Sánchez, M. A., Cyran, J. D., Kiselev, A., and Bonn, M.: Surface charge-induced orientation of interfacial water suppresses heterogeneous ice nucleation on α-alumina (0001), Atmos. Chem. Phys. Discuss., 2017, 1-13, doi: 10.5194/acp-2017-224, 2017.

Anim-Danso, E., Zhang, Y., and Dhinojwala, A.: Surface Charge Affects the Structure of Interfacial Ice, J. Phys. Chem. C, 120, 3741-3748, doi: 10.1021/acs.jpcc.5b08371, 2016.

Balmer, T. E., Christenson, H. K., Spencer, N. D., and Heuberger, M.: The Effect of Surface Ions on Water Adsorption to Mica, Langmuir, 24, 1566-1569, doi: 10.1021/la702391m, 2008.

Baron, P. A. and Willeke, K.: Aerosol Measurement: Principles,Techniques, and Applications, 2 ed., edited by: Sons, J., Wiley-Interscience, 2001.

5 Beaglehole, D., Radlinska, E. Z., Ninham, B. W., and Christenson, H. K.: Inadequacy of Lifshitz theory for thin liquid films, Phys. Rev. Lett., 66, 2084-2087, 1991.

Campbell, J. M., Meldrum, F. C., and Christenson, H. K.: Characterization of Preferred Crystal Nucleation Sites on Mica Surfaces, Cryst. Growth Des., 13, 1915-1925, doi: 10.1021/cg301715n, 2013.

Christenson, H. K. and Israelachvili, J. N.: Growth of ionic crystallites on exposed surfaces, J. Colloid. Interface. Sci., 117, 576-577, doi: 10 10.1016/0021-9797(87)90420-6, 1987.

Christenson, H. K. and Thomson, N. H.: The nature of the air-cleaved mica surface, Surf. Sci. Rep., 71, 367-390, doi: 10.1016/j.surfrep.2016.03.001, 2016.

DeMott, P. J., Möhler, O., Stetzer, O., Vali, G., Levin, Z., Petters, M. D., Murakami, M., Leisner, T., Bundke, U., Klein, H., Kanji, Z. A., Cotton, R., Jones, H., Benz, S., Brinkmann, M., Rzesanke, D., Saathoff, H., Nicolet, M., Saito, A., Nillius, B., Bingemer, H., 15 Abbatt, J., Ardon, K., Ganor, E., Georgakopoulos, D. G., and Saunders, C.: Resurgence in Ice Nuclei Measurement Research, Bull. Am. Meteorol. Soc., 92, 1623-1635, doi: 10.1175/2011bams3119.1, 2011.

Eastwood, M. L., Cremel, S., Gehrke, C., Girard, E., and Bertram, A. K.: Ice nucleation on mineral dust particles: Onset conditions, nucleation rates and contact angles, J. Geophys. Res.: Atmospheres, 113, 203-201 - 203-209, doi: 10.1029/2008jd010639, 2008.

Fordyce, A. J., Bullock, W. J., Timson, A. J., Haslam, S., Spencer-Smith, R. D., Alexander, A., and Frey, J. G.: The temperature 20 dependence of surface second-harmonic generation from the air-water interface, Mol. Phys., 99, 677-687, doi: 10.1080/00268970010030022, 2001.

Goh, M. C., Hicks, J. M., Kemnitz, K., Pinto, G. R., Heinz, T. F., Eisenthal, K. B., and Bhattacharyya, K.: Absolute orientation of water molecules at the neat water surface, J. Phys. Chem., 92, 5074-5075, doi: 10.1021/j100329a003, 1988.

Hinds, W. C.: Aerosol Technology: Properties, Behavior, and Measurement of Airborne Particles, 2 ed., Wiley-Interscience, 1999.

25 Hoose, C. and Mohler, O.: Heterogeneous ice nucleation on atmospheric aerosols: a review of results from laboratory experiments, Atmos. Chem. Phys., 12, 9817-9854, doi: 10.5194/acp-12-9817-2012, 2012.

Hu, J., Xiao, X.-D., Ogletree, D. F., and Salmeron, M.: Imaging the Condensation and Evaporation of Molecularly Thin Films of Water with Nanometer Resolution, Science, 268, 267-269, doi: 10.1126/science.268.5208.267, 1995.

Jang, J. H., Lydiatt, F., Lindsay, R., and Baldelli, S.: Quantitative Orientation Analysis by Sum Frequency Generation in the Presence of 30 Near-Resonant Background Signal: Acetonitrile on Rutile TiO2 (110), J. Phys. Chem. A, 117, 6288-6302, doi: 10.1021/jp401019p, 2013.

Kiselev, A., Bachmann, F., Pedevilla, P., Cox, S. J., Michaelides, A., Gerthsen, D., and Leisner, T.: Active sites in heterogeneous ice nucleation—the example of K-rich feldspars, Science, doi: 10.1126/science.aai8034, 2016.

Layton, R. G. and Harris, F. S.: Nucleation of Ice on Mica, J. Atmos. Sci., 20, 142-148, doi: 10.1175/1520-35 0469(1963)020<0142:noiom>2.0.co;2, 1963.

Libbrecht, K.: Growth rates of the principal facets of ice between −10°C and −40°C, Journal of Crystal Growth, 247, 530-540, doi: https://doi.org/10.1016/S0022-0248(02)01996-6, 2003.

Libbrecht, K. G.: The physics of snow crystals, Rep. Prog. Phys, 68, 855, doi: 10.1088/0034-4885/68/4/R03, 2005.

Lovering, K. A., Bertram, A. K., and Chou, K. C.: Transient Phase of Ice Observed by Sum Frequency Generation at the Water/Mineral 40 Interface During Freezing, J. Phys. Chem. Lett., 8, 871-875, doi: 10.1021/acs.jpclett.6b02920, 2017.

Luca, A. A. T., Hebert, P., Brevet, P. F., and Girault, H. H.: Surface second-harmonic generation at air/solvent and solvent/solvent interfaces, J. Chem. Soc. Faraday Trans., 91, 1763-1768, doi: 10.1039/ft9959101763, 1995.

Lupi, L., Kastelowitz, N., and Molinero, V.: Vapor deposition of water on graphitic surfaces: Formation of amorphous ice, bilayer ice, ice I, and liquid water, J. Chem. Phys., 141, 18C508, doi: 10.1063/1.4895543, 2014.

45 Mason, B. J. and Maybank, J.: Ice-nucleating properties of some natural mineral dusts, Q. J. R. Meteorol. Soc., 84, 235-241, doi: 10.1002/qj.49708436104, 1958.

Odelius, M., Bernasconi, M., and Parrinello, M.: Two Dimensional Ice Adsorbed on Mica Surface, Phys. Rev. Lett., 78, 2855-2858, doi: 10.1103/PhysRevLett.78.2855, 1997.

Ong, S., Zhao, X., and Eisenthal, K. B.: Polarization of water molecules at a charged interface: second harmonic studies of the silica/water 50 interface, Chem. Phys. Lett., 191, 327-335, doi: 10.1016/0009-2614(92)85309-X, 1992.

Ostendorf, F., Schmitz, C., Hirth, S., Kühnle, A., Kolodziej, J. J., and Reichling, M.: How flat is an air-cleaved mica surface?, Nanotechnology, 19, 305705, doi: 10.1088/0957-4484/19/30/305705, 2008.

Poppa, H. and Elliot, A. G.: The surface composition of Mica substrates, Surf. Sci., 24, 149-163, doi: 10.1016/0039-6028(71)90225-1, 1971.

55 Pruppacher, H. R. and Klett, J. D.: Microphysics of clouds and precipitation, 2 ed., Atmospheric and oceanographic sciences library, 18, Kluwer Academic Publishers, Dordrecht ; Boston, 954 pp., 1997.

Rao, Y., Tao, Y.-s., and Wang, H.-f.: Quantitative analysis of orientational order in the molecular monolayer by surface second harmonic generation, J. Chem. Phys., 119, 5226-5236, doi: 10.1063/1.1597195, 2003.

Schaefer, V. J.: The Formation of Ice Crystals in the Laboratory and the Atmosphere, Chem. Rev., 44, 291-320, doi: 60 10.1021/cr60138a004, 1949.

Shen, Y. R.: Optical Second Harmonic Generation at Interfaces, Annu. Rev. Phys. Chem., 40, 327-350, doi: 10.1146/annurev.pc.40.100189.001551, 1989a.

Shen, Y. R.: Surface properties probed by second-harmonic and sum-frequency generation, Nature, 337, 519-525, doi: 10.1038/337519a0, 1989b.

65 Slater, B., Michaelides, A., Salzmann, C. G., and Lohmann, U.: A Blue-Sky Approach to Understanding Cloud Formation, Bull. Am. Meteorol. Soc., 97, 1797-1802, doi: 10.1175/bams-d-15-00131.1, 2016.

Willeke, K. and Baron, P.: Aerosol Measurement: Principles, Techniques, and Applications, edited by: Klaus Willeke, P. A. B., Van Nostrand Reinhold, 1993.

Zhang, L., Tian, C., Waychunas, G. A., and Shen, Y. R.: Structures and Charging of α-Alumina (0001)/Water Interfaces Studied by Sum-70 Frequency Vibrational Spectroscopy, J. Am. Chem. Soc., 130, 7686-7694, doi: 10.1021/ja8011116, 2008.

Zhao, X., Ong, S., and Eisenthal, K. B.: Polarization of water molecules at a charged interface. Second harmonic studies of charged monolayers at the air/water interface, Chem. Phys. Lett., 202, 513-520, doi: 10.1016/0009-2614(93)90041-X, 1993.

Zhuang, X., Miranda, P. B., Kim, D., and Shen, Y. R.: Mapping molecular orientation and conformation at interfaces by surface nonlinear optics, Phys. Rev. B, 59, 12632-12640, doi: 10.1103/PhysRevB.59.12632, 1999.

1 **Supporting information (SI) for: Direct molecular level characterization of different heterogeneous**
2 **freezing modes on mica – Part 1**

3 Ahmed Abdelmonem[1]

4 [1]Institute of Meteorology and Climate Research – Atmospheric Aerosol Research (IMKAAF), Karlsruhe
5 Institute of Technology (KIT), 76344 Eggenstein-Leopoldshafen, Germany

6 Correspondence to: Ahmed Abdelmonem (ahmed.abdelmonem@kit.edu)

7

8 **Abbreviations**

9 SHG: second-harmonic generation,

10 SFG: sum-frequency generation

11 IMG: index-matching gel

12 TIR: total internal reflection

13 RH: relative humidity

14

15

1 SFG and SHG: Theoretical background

2 SFG and SHG are highly sensitive nonlinear optical probes of surfaces and interfaces where light is
3 generated at a frequency equals to the sum of frequencies of two incident optical fields. The basic
4 theory of SHG and SFG has been described elsewhere (Bain, 1995; Eisenthal, 1996; Richmond et al.,
5 1988; Shen, 1989a; Shen, 1989b; Shen, 1994; Shen and Ostroverkhov, 2006) and will not be repeated
6 here. However, a brief background will be given here. SFG/SHG signal is generated when the incident
7 beams are spatially and temporally overlapped at a point of broken inversion-symmetry (e.g. an
8 interface between two isotropic media). The experiments are usually carried out with definite
9 polarization combinations of incident and generated beams. Such experiments are rich of
10 information, particularly about concentrations and orientations of the entities which contribute to
11 the signal. Unlike SHG, SFG can specify the different entities from their resonance frequencies. SHG
12 and SFG have been used to probe the aqueous/air, aqueous/solid and solid/air interfaces. The overall
13 signal strength depends on 1) intensity and polarization of the incident beams, 2) the optical
14 properties of the media at the interface manifested in the Fresnel factors and 3) the concentrations
15 and orientations of the molecules and the response of the existing dipoles at the interface.

16 Generally the SFG signal, of frequency $\omega_{SF} = \omega_v + \omega_{IR}$, generated at the interface, Figure (S1), is
17 given as bellow:

$$I(\omega_{SF}) \propto \left| L(\omega_{SF})\, \chi^{(2)}\, L(\omega_v).\, L(\omega_{IR}) \right|^2 I_v I_{IR} \qquad (1)$$

18 where, $L(\omega_i)$ is the nonlinear Fresnel factor at ω_i and $\chi^{(2)}$ is the second order nonlinear
19 hyperpolarizability tensor. ω_v and ω_{IR} are the frequencies of the incident beams. In SHG, the two
20 incident frequencies are equal. Polarization dependent measurements probe specific tensor element
21 of the hyperpolarizability tensor and yield detailed information about the degree of ordering and
22 angular orientation of the molecules (Abdelmonem, 2008; Shen, 1989a; Shen, 1989b; Jang et al.,
23 2013; Rao et al., 2003; Zhuang et al., 1999; Fordyce et al., 2001; Goh et al., 1988; Luca et al., 1995).
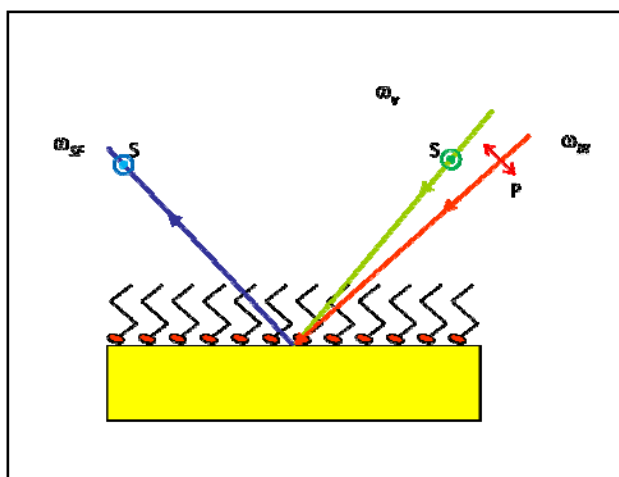

24

25 **Figure S1: Simple scheme of SFG generation in co-propagating geometry. S and P indicate light polarized light**
26 **perpendicular and parallel to the plane of incidence respectively.**

27

1   **Data acquisition and Fresnel factors correction (SHG)**

2   - *Data acquisition*

3   During the SHG experiments the signal was collected, averaged and stored as a function of the state
4   of condensation, deposition, freezing, or formation of bulk. These are the data points plotted in Figs.
5   3 and 4 in the manuscript. Only for Fig. 5 the data was recorded as a function of time to report on the
6   detected transient ice formed upon immersion freezing. Figure S2, shows some screen shots of
7   typical SHG signal and temperature changes in time, and shows the points where the signal was
8   collected and averaged for Figs. 3 and 4.
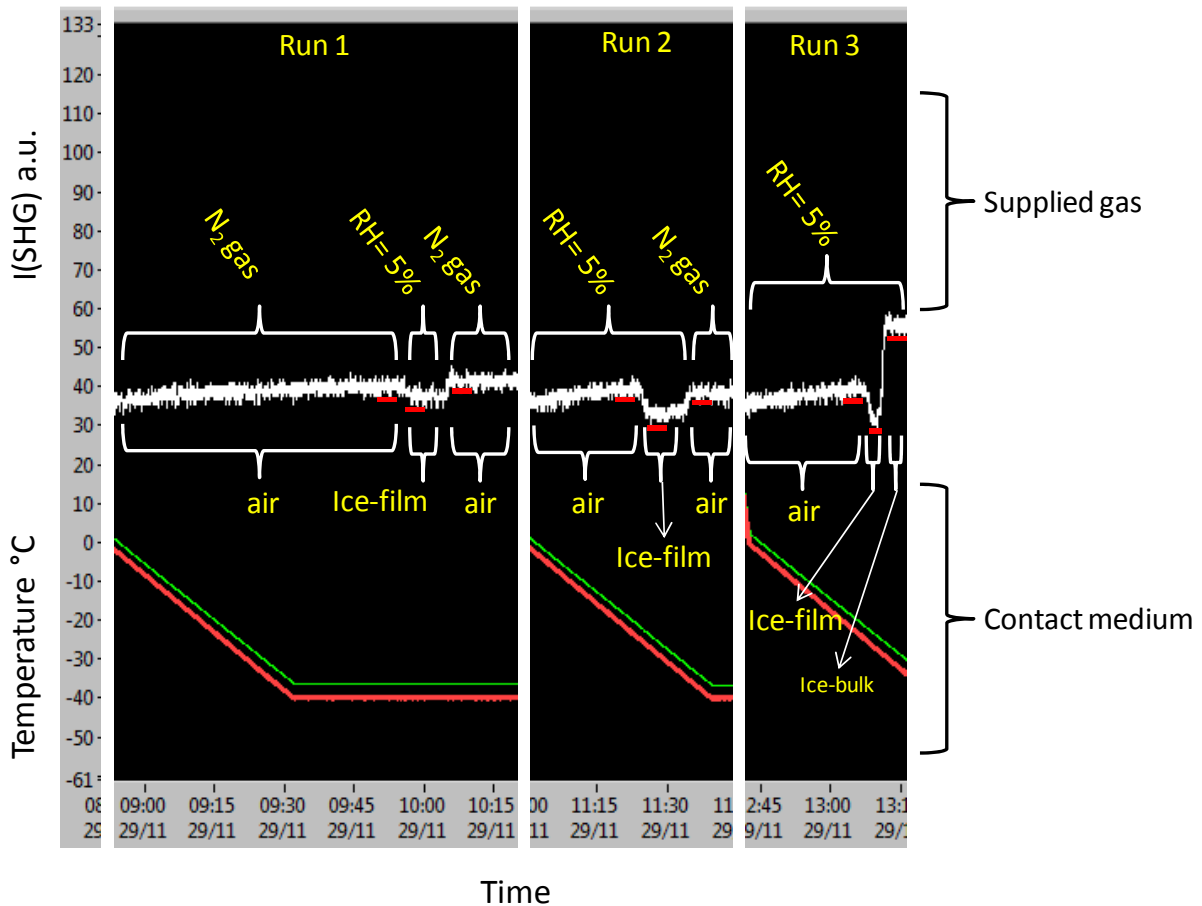
9

10   **Figure S2: Screen shots of typical signal and temperature changes in time during arbitrary cooling processes. The white**
11   **line shows raw SHG data. The short red dashes below the SHG data show the points where the signal was collected and**
12   **averaged. The red and green lines show the temperatures of the sample bottom and sample top respectively.**

13   Figure S2 shows three examples of three arbitrary runs performed on sapphire (only for
14   demonstration purpose):

15   Run1: The cell was purged continuously with N_2 gas while cooling the sample down to -40. There is a
16   small gradual change in the signal due to the changes in the temperature dependent optical
17   constants. The cell was then purged with humid air which resulted in a formation of an ice-film by
18   deposition. Finally, the cell was purged again with N_2 gas which resulted in sublimation of the ice
19   film.

20   Run2: The cell was purged with humid air (RH=5%) while cooling the sample down until the
21   formation of an ice film and then the cell was purged by N_2 gas which resulted in film sublimation.

3

1 Run3: The cell was purged with humid air (RH=5%) while cooling the sample down until the
2 formation of an ice film. Purging the cell with humid air was continued until the formation of bulk ice.

3 All experiments of deposition freezing were done in a similar way as described above. Figs. 3 and 4 in
4 the manuscript show the averaged signal at each event and the error bars on the figures show the
5 fluctuation in the data points among all repeated experiments.

6

7 - *Fresnel factors*

8 The SHG signal with a frequency $\omega_{SH} = 2\omega_{in}$ under SM polarization, (S-polarized SHG and 45°-
9 polarized incident light), generated from an incoming visible light with a frequency ω_{in} can be
10 described with the equation:

$$S_{SM}(\omega_{SH}) \propto \left| L_{yy}(\omega_{SH})L_{yy}(\omega_{in})L_{zz}(\omega_{in})\chi_{yyz}^{(2)} \right|^2 I_{in}^2 \tag{2}$$

11 where, $L(\omega_i)$ is the nonlinear Fresnel factor at ω_i and $\chi_{yyz}^{(2)}$ is the surface second order nonlinear
12 susceptibility tensor for SM polarisation combination (equivalent to SSP in SFG) (Shen, 1989b; Zhuang
13 et al., 1999) and a measure of the degree of molecular ordering. To obtain the molecular quantity
14 $\chi_{yyz}^{(2)}$ the measured SHG intensities have thus to be normalized to the Fresnel factors which are
15 optical constants dependent. Figure S3 shows the change of Fresnel factors as a function of refractive
16 index in the range of refractive indices covering the involved media in this work. The SHG intensities
17 reported in Figures 3 and 4 in the manuscript are Fresnel corrected and thus directly proportional
18 to $\left| \chi_{yyz}^{(2)} \right|^{(2)}$.
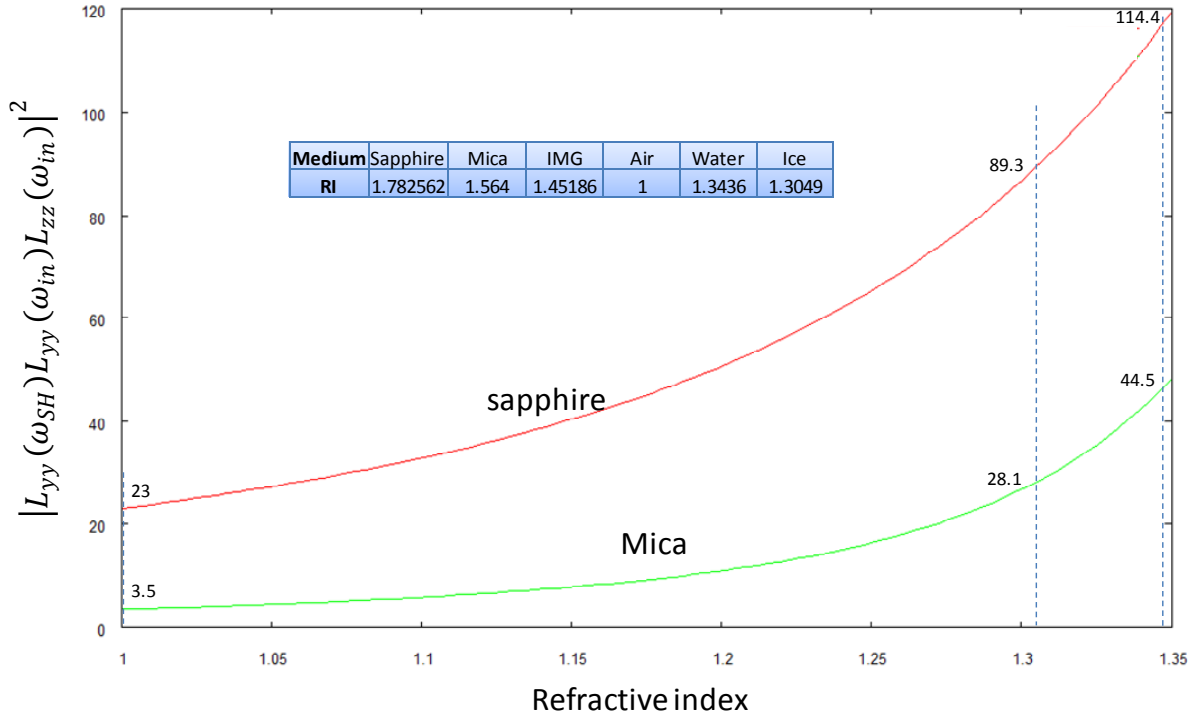
| Medium	Sapphire	Mica	IMG	Air	Water	Ice
RI	1.782562	1.564	1.45186	1	1.3436	1.3049

20 **Figure S3: Theoretically calculated Fresnel factors for sapphire-water (red line) and mica-water (green line)**
21 **interfaces at incident angle of 15° from air to the sapphire prism. Optical geometry can be found in (Abdelmonem et**
22 **al., 2015; Abdelmonem et al., 2017).**

1

The Fresnel factors are expected to change with temperature and hence affect the measured SHG signal. The influence of the temperature dependence of the optical properties of the IMG, sapphire prism and mica on the SHG signal was studied before starting the series of measurements. Figure S4 shows the SHG at mica-N_2 gas interface in the mentioned range of temperatures. There was no significant effect of the changes in the optical properties of these media on the detected signal within the range of freezing temperatures observed in the study.

8
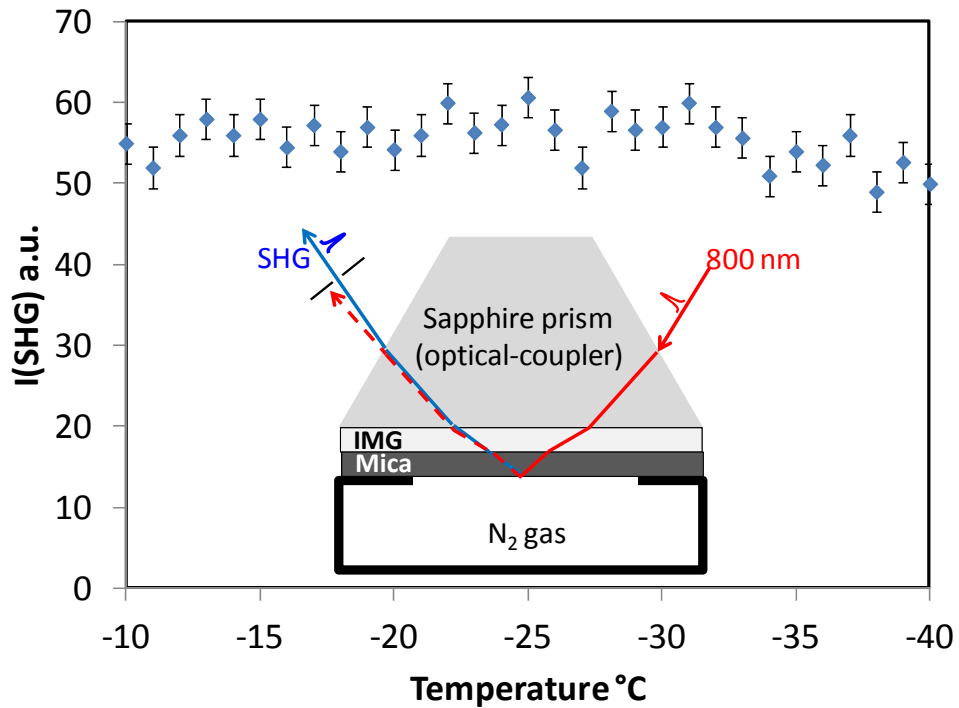
Figure S4: SHG at mica-N_2 gas interface in the range of freezing temperatures observed in the study. The cell, shown in Figure 2, was filled with ultrapure N_2 gas (99.9999 %).

11

12

References

Abdelmonem, A.: Nonlinear optical spectroscopy at the Liquid-/Solid- interface, 1.0, Naturwissenschaften, Mathematik und Informatik, Ruprecht – Karls – Universität, Heidelberg, 2008.

Abdelmonem, A., Lützenkirchen, J., and Leisner, T.: Probing ice-nucleation processes on the molecular level using second harmonic generation spectroscopy, Atmos. Meas. Tech., 8, 3519-3526, doi: 10.5194/amt-8-3519-2015, 2015.

Abdelmonem, A., Backus, E. H. G., Hoffmann, N., Sánchez, M. A., Cyran, J. D., Kiselev, A., and Bonn, M.: Surface charge-induced orientation of interfacial water suppresses heterogeneous ice nucleation on α-alumina (0001), Atmos. Chem. Phys. Discuss., 2017, 1-13, doi: 10.5194/acp-2017-224, 2017.

Bain, C. D.: Sum-frequency vibrational spectroscopy of the solid/liquid interface, J. Chem. Soc. Faraday Trans., 91, 1281-1296, doi: 10.1039/ft9959101281, 1995.

Eisenthal, K. B.: Liquid Interfaces Probed by Second-Harmonic and Sum-Frequency Spectroscopy, Chem. Rev., 96, 1343-1360, doi: 10.1021/cr9502211, 1996.

Fordyce, A. J., Bullock, W. J., Timson, A. J., Haslam, S., Spencer-Smith, R. D., Alexander, A., and Frey, J. G.: The temperature dependence of surface second-harmonic generation from the air-water interface, Mol. Phys., 99, 677-687, doi: 10.1080/00268970010030022, 2001.

Goh, M. C., Hicks, J. M., Kemnitz, K., Pinto, G. R., Heinz, T. F., Eisenthal, K. B., and Bhattacharyya, K.: Absolute orientation of water molecules at the neat water surface, J. Phys. Chem., 92, 5074-5075, doi: 10.1021/j100329a003, 1988.

Jang, J. H., Lydiatt, F., Lindsay, R., and Baldelli, S.: Quantitative Orientation Analysis by Sum Frequency Generation in the Presence of Near-Resonant Background Signal: Acetonitrile on Rutile TiO2 (110), J. Phys. Chem. A, 117, 6288-6302, doi: 10.1021/jp401019p, 2013.

Luca, A. A. T., Hebert, P., Brevet, P. F., and Girault, H. H.: Surface second-harmonic generation at air/solvent and solvent/solvent interfaces, J. Chem. Soc. Faraday Trans., 91, 1763-1768, doi: 10.1039/ft9959101763, 1995.

Rao, Y., Tao, Y.-s., and Wang, H.-f.: Quantitative analysis of orientational order in the molecular monolayer by surface second harmonic generation, J. Chem. Phys., 119, 5226-5236, doi: 10.1063/1.1597195, 2003.

Richmond, G. L., Robinson, J. M., and Shannon, V. L.: Second harmonic generation studies of interfacial structure and dynamics, Prog. Surf. Sci., 28, 1-70, doi: 10.1016/0079-6816(88)90005-6, 1988.

Shen, Y. R.: Surface properties probed by second-harmonic and sum-frequency generation, Nature, 337, 519-525, doi: 10.1038/337519a0, 1989a.

Shen, Y. R.: Optical Second Harmonic Generation at Interfaces, Annu. Rev. Phys. Chem., 40, 327-350, doi: 10.1146/annurev.pc.40.100189.001551, 1989b.

Shen, Y. R.: Surfaces probed by nonlinear optics, Surf. Sci., 299, 551-562, doi: 10.1016/0039-6028(94)90681-5, 1994.

Shen, Y. R. and Ostroverkhov, V.: Sum-Frequency Vibrational Spectroscopy on Water Interfaces: Polar Orientation of Water Molecules at Interfaces, Chem. Rev., 106, 1140-1154, doi: 10.1021/cr040377d, 2006.

Zhuang, X., Miranda, P. B., Kim, D., and Shen, Y. R.: Mapping molecular orientation and conformation at interfaces by surface nonlinear optics, Phys. Rev. B, 59, 12632-12640, doi: 10.1103/PhysRevB.59.12632, 1999.